Instruments and Methods

An improved transient-type ice-penetrating radar

Shengbo YE,[1,2] Bin ZHOU,[1,2] Bingheng WU,[1,2] Bo ZHAO,[1] Guangyou FANG[1]

[1]*Key Laboratory of Electromagnetic Radiation and Detection Technology, Institute of Electronics, Chinese Academy of Sciences, Beijing 100190, China*
E-mail: gyfang@mail.ie.ac.cn
[2]*Graduate University of Chinese Academy of Sciences, Beijing 100190, China*

ABSTRACT. A low-cost, compact, short-pulse ice-penetrating radar (IPR) system with a center frequency of 50 MHz for sounding glacier topography is presented. The radar was developed to measure ice thickness and to image internal structures and basal conditions of glaciers and ice sheets with a maximum range of ~16 000 ns and a depth resolution better than 2.5 m. The receiver of the IPR system employs asynchronous operation mode, avoiding the need for a cable between the transmitter and receiver. A new sampling technology using a high-speed field programmable gate array, which implements a 256-trace stacking algorithm to realize the analog-to-digital conversion, both simplifies the structure of the receiver and increases the sampling efficiency. The power consumption of the whole receiver is <1.5 W, which can be supplied by a laptop computer. Test measurements were made during the 5th China Expedition to the Grove Mountains in East Antarctica. Field tests show the capability of this system to measure ice thickness up to 650 m and to define internal layers within the ice body.

INTRODUCTION

Ice-penetrating radar (IPR) is an efficient and common geophysical tool in glaciology (Bogorodsky and others, 1985), with applications including ice depth sounding (Sverrisson and others, 1980), ice-sheet stratigraphy mapping (Nereson and others, 2000) and englacial (Catania and others, 2008) and subglacial (Jacobel and others, 2009) condition studies. Surface-based radars capable of reaching 3–4 km depth with interface resolution of a few meters are needed for englacial studies of strata, flow dynamics and deep ice-core site selection. This resolution is required to determine whether small-scale nonconformities exist, the nature of folds, etc. Currently, such radars operate at 1–15 MHz and can therefore sense the bottom with interface resolution of tens of meters. Airborne systems operating at 50 MHz and higher easily profile the bed, but their pulse waveforms consist of many cycles, thus losing the advantage of high resolution that a ground-based pulse system can provide. In this paper, we discuss development of a 50 MHz surface-based short-pulse radar.

There have been several studies of surface pulsed IPR system design over the past tens of years. Jones and others (1989) designed a portable, digital pulse radar with center frequency of 15 MHz in air. Their system had a total weight of 7.9 kg and power consumption of 17 W. The peak pulse amplitude was ~1200 V, and the resolution and sampling rate of the receiver were 8 bits and 102 MHz respectively. In ice, the depth resolution of this system was ~8 m and the maximal penetrating range was ~841 m. Wright and others (1990) developed a digital low-frequency surface-profiling ice radar, which operated at 1, 2, 4, 8 and 12.5 MHz. The resolution and sampling rate of the receiver were 8 bits and 100 MHz respectively. The depth resolution of this system was <10 m in ice. It obtained 800 m penetrating range at 2 MHz. Since 2000, Welch and Jacobel have conducted many measurements in Antarctica using IPR systems (Welch and Jacobel, 2003, 2005; Welch and others, 2009) at 3 MHz frequency, resulting in a depth resolution of ~40 m. The receivers of their recent systems have 14-bit accuracy with 100 MHz sampling rate and penetration range of 3–4 km. Conway and others (2009) developed a pulse radar system operating at 2 MHz. The peak pulse amplitude was ~±2000 V. The resolution and sampling rate of the receiver were 14 bits and 100 MHz respectively. The depth resolution of this system was <62.5 m in ice. It detected the bed through ice up to 1250 m thick. Mingo and Flowers (2010) developed an integrated, lightweight radar operating at 10.5 and 5 MHz. The depth resolution of their system was <12 m in ice. The radar transmit pulse had peak amplitude 1100 V and achieved 220 m penetration range at 10.5 MHz and 550 m penetration range at 5 MHz. Other commercial systems (e.g. the Sensors and Software pulseEKKO) advertise a range of ~10 000 ns and depths up to 800 m in ice, but this has not yet been achieved in the field. Though the radars above may attain a penetration range of thousands of meters, they suffer low depth resolution and high power consumption. Radars exhibiting high resolution, large penetration range, low power consumption and low weight are required for most glacier topography applications.

We present a low-cost, compact, short-pulse IPR system with a center frequency of 50 MHz for sounding glacier topography. To achieve a high penetration range, the peak amplitude of the short pulse is increased to ±2500 V. The receiver of the IPR system operates asynchronously, avoiding the need for a cable between the transmitter and receiver. Furthermore, we use a new sampling technology without integrated analog-to-digital conversion to simplify the structure of the receiver and increase the sampling efficiency. The new sampling technology implements a 256-trace stacking algorithm to realize the analog-to-digital conversion by using a high-speed field programmable gate array (FPGA). The IPR system has a sampling rate of 512 MHz with 8-bit accuracy and a maximum range of ~16 000 ns. The total weight of the system is ~4.2 kg. Our

https://doi.org/10.3189/002214311796405861 Published online by Cambridge University Press

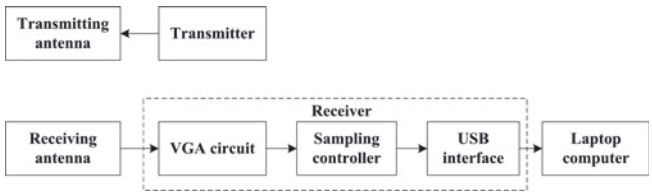

Fig. 1. Block diagram of our IPR system.

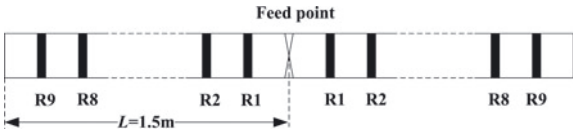

Fig. 2. The structure of a discrete resistively loaded dipole wire antenna. The total length for a 50 MHz antenna is ~3 m.

objectives are to achieve a depth range >800 m in cold ice and a depth resolution better than 2.5 m.

We carried out several test measurements in the region of the Grove Mountains (72°20′–73°10′ S, 73°50′–75°40′ E), located ~400 km inland (south) of the Larsemann Hills, Princess Elizabeth Land, East Antarctica. This is the first time China has used an independently developed IPR system to map ice thickness, internal structure and basal conditions of glaciers and ice sheets. We present technical details of the IPR system, including transmitter, antenna and receiver. Typical measurement results from our test profiles are provided, showing ice thickness up to 650 m and internal layers.

SYSTEM DESIGN

The block diagram of the developed IPR system is shown in Figure 1. It consists of a transmitter, a receiver, transmit and receive antennas and a laptop computer. In order to improve the performance of the receiver, a variable-gain amplifier (VGA) circuit is used before the receiver. Unlike the operation mode of conventional radar in which the transmitter is triggered by the receiver, the transmitter radiates pulses in asynchronous mode so that the transmitter and receiver have no electrical coupling, thus avoiding interference caused by the usual cable between the transmitter and the receiver. The characteristics of the asynchronous mode are that the transmitter transmits pulses without the trigger signal from the receiver or controller (Welch and Jacobel, 2003) and the receiver automatically extracts the synchronous signal from the input echoes, like a real-time oscilloscope. This mode is quite useful in low-frequency radar application where a large distance is required between the transmitter and the receiver. Because there is no trigger cable, field measurement is more convenient, especially in the harsh polar environment. The radar system component characteristics for hand-towed implementation are described in Table 1.

Table 1. The radar system component characteristics for hand-towed implementation.

Component	Dimensions	Weight	Power consumption
	cm	kg	W
Transmitter (incl. 12 V battery and metal box)	20 × 12 × 6.5	1.94	<0.1
Receiver (incl. metal box)	18.5 × 12 × 6.5	1.37	<1.5
Tx/Rx antennas	150 half-length	0.5 each	

Transmitter

The transmitter, which is powered by a 12 V battery, employs spark-gap to provide sufficient power to survey ice depths of several hundred meters in both cold and temperate glaciers. The transmitter with battery and metal box is small (1.94 kg), making it ideally suited for surveys without vehicular support. The transmitter delivers 5000 V (±2500 V) pulses into 50 Ω across a resistively loaded dipole antenna. It has a rise time of <2 ns and can operate within a 1–200 MHz frequency range. Since the transmitter generates a short pulse with a broad frequency spectrum, the peak radiated frequency depends on the characteristics of the transmit antenna (Conway and others, 2009).

Generally, for short-pulse radar, the shape of the pulse from the transmitter is approximately Gaussian. After the pulse has traveled though the transmitter and receiver antennas, its shape is approximately that of a Ricker wavelet, i.e. the second differential of a Gaussian function, whose envelope remains a Gaussian waveform. A theoretical depth resolution, an important value for the investigation of internal ice layers, can be calculated by means of the definition of radar resolution. The relationship between the vertical interface resolution, δ, the system bandwidth, B, and propagation velocity of the radar signal in cold ice, v, is

$$\delta = \frac{v}{2B}. \quad (1)$$

In general, the propagation velocity of the electromagnetic wave in cold ice is $\sim 168 \times 10^6\ \mathrm{m\,s^{-1}}$ (Bogorodsky and others, 1985). After power on, the transmitter automatically generates a single-cycle short pulse at the pulse repetition frequency (PRF) of 1 kHz.

Transmitter and receiver antennas

In order to obtain high isolation of near-interface layers, separate antennas for transmission and reception are needed. The performance of the transmitter and receiver (T/R) antenna pair strongly affects the IPR performance. Because of the low level of any ringing, resistively loaded dipole antennas are employed in the IPR system. We designed our resistor values according to Wu and King's (1965) loaded-resistance formula,

$$Z(x) = \frac{K}{L - |x|}\,(\Omega\,\mathrm{m^{-1}}), \quad (2)$$

where x is the distance along the arm from the feed point of the antenna, L is the length of the arm, and K is a constant mainly dependent on the intrinsic impedance of the dipole antennae.

In order to improve the penetrating ability of the electromagnetic wave, the center frequency of the antennae is ~50 MHz in air. Figure 2 shows the structure of the discrete resistively loaded dipole wire antenna. From Equation (2), the specific discrete loaded resistance formula is

https://doi.org/10.3189/002214311796405861 Published online by Cambridge University Press

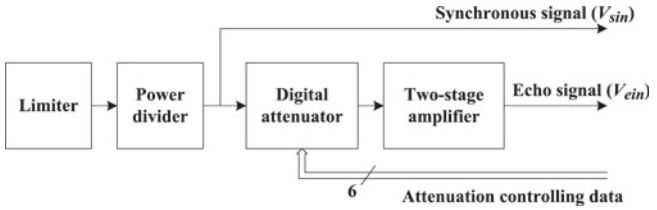

Fig. 3. Block diagram of the VGA circuit.

given by

$$R_i = \frac{Rl}{L - |x_i|}, \quad i = 1, 2..., 9, \tag{3}$$

where R is resistance of the tip-loaded resistor which is generally 200 Ω, l is the distance to the neighboring loaded resistor and x_i is the distance to the ith loaded resistor along the arm from the feed point of the antenna.

Variable-gain amplifier circuit

The block diagram of the VGA circuit is shown in Figure 3 and consists of a limiter, a power divider, a 6-bit digital attenuator and a two-stage amplifier. The VGA circuit improves signal-to-noise ratio and the dynamic range of the receiver. Because the direct wave that reflects from the air/ground interface is much stronger than any subsurface signal, we used a limiter to clip the direct wave to protect the following components. A power divide circuit divided the input signal into two parts, one fed to a sampling control circuit as a synchronous signal, V_{sin}, and the other to the digital attenuator. The digital attenuator has a maximal 50 dB total attenuation range with a 1 dB minimum step size. The attenuation change can be performed by the sampling-controlling circuits. After attenuation, the signal is amplified ~50 dB by a two-stage amplifier and then fed to the sampling control circuit as the final received echo signal, V_{ein}.

Sampling controller

Conventional equivalent-time sampling technology uses thousands of echoes to reconstruct the original radar echo trace, leading to low echo utilization. Real-time sampling technology uses high-speed analog-to-digital conversion with >500 MHz sampling rate, leading to high cost and complicated circuit structure. We present a novel sampling controller which employs a high-speed FPGA to realize equivalent 8-bit accuracy at 512 MHz sampling rate without using integrated analog-to-digital conversion, resulting in low power consumption and simplified circuit structure. Furthermore, we need only 256 radar echoes to realize an A-SCAN reconstruction independent of the number of sample points. Nearly all the functions (e.g. data acquisition, control tasks and communication tasks) are implemented in the FPGA and they can be changed flexibly within the FPGA software. The block diagram of the sampling-controlling circuit (Fig. 4) consists of an 8-bit digital-to-analog converter (DAC) and a FPGA (xc3s400-4PQ208, Xilinx Inc.). We use the low-voltage positive emitter-coupled logic (LVPECL) standard differential input buffer of the FPGA as analog comparator.

The echo signal, V_{ein}, is first given an appropriate fixed bias voltage, $V_{\text{ein\_DC}}$, and then applied to the positive input of one differential input buffer (Buffer_e). The output of the

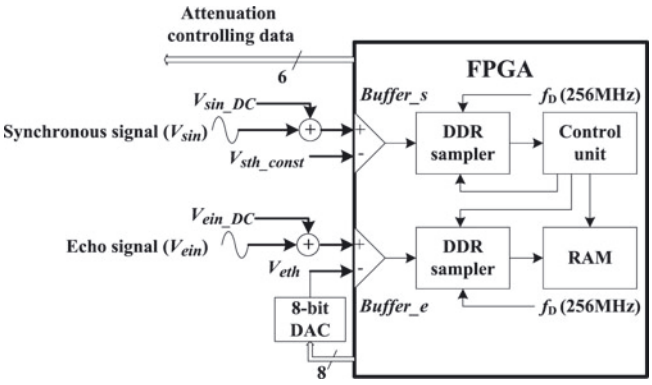

Fig. 4. Block diagram of the sampling controller.

low-speed DAC, V_{eth}, is applied to the negative input as reference voltage. A double data rate (DDR) sampler, whose operation frequency is f_{D} (256 MHz), samples the output of Buffer_e. The Buffer_e, the DAC and the DDR sampler make up a 1-bit real-time sampling analog-to-digital converter with 512 MHz sampling rate. During one echo, all the M sample points needed are quantified to 1-bit digital words in $M/2$ consecutive clock cycles of the DDR sampler. For the nth echo, where $n = 1, 2, ..., 256$, we define the nth-step V_{eth} by $V_{\text{eth}}(n)$, which satisfies

$$V_{\text{eth}}(n) = V_{\text{init}} + (n-1) \cdot \Delta v, \tag{4}$$

where V_{init} is the first step of V_{eth} and Δv is the quantified level at ~2.3 mV. Generally, $V_{\text{ein\_DC}}$ should be approximately equal to $V_{\text{eth}}(128)$ or $V_{\text{eth}}(129)$.

We also define the 1-bit quantified result of the mth sample point by $S_n(m)$, corresponding to $V_{\text{eth}}(n)$, where $m = 1, 2, ..., M$:

$$S_n(m) = \begin{cases} 1, & \text{for } (V_{\text{ein}} + V_{\text{ein\_DC}}) > V_{\text{eth}}(n) \\ 0, & \text{otherwise} \end{cases}. \tag{5}$$

After 1-bit conversions have been carried out 256 times, we obtain a bitmap matrix, $B_{256\times M}$, in which every element is either '1' or '0':

$$B_{256\times M} = \begin{pmatrix} S_1(m) \\ S_2(m) \\ \vdots \\ S_{256}(m) \end{pmatrix}. \tag{6}$$

The equivalent 8-bit digital value of all M sample points can be calculated by

$$y(m) = \sum_{n=1}^{256} S_n(m). \tag{7}$$

This process can reduce the effect of the noise and is done on a laptop computer in the field.

Though some commercial systems such as those of Geophysical Survey Systems Inc. (GSSI) and Sensors and Software have the advantage of accuracy and sampling rate, they use an analog sampling gate to convert signals to audio range. This process may lose some information (Tsui and Stephens, 2002). Compared with these commercial systems, our system has no analog sampling gate or analog-to-digital conversion, and integrates the analog-to-digital circuit and the control circuit together to form a cohesive whole. Though this system has only 8-bit accuracy, the quantification level, ~2.3 mV, does not degrade performance significantly and

https://doi.org/10.3189/002214311796405861 Published online by Cambridge University Press

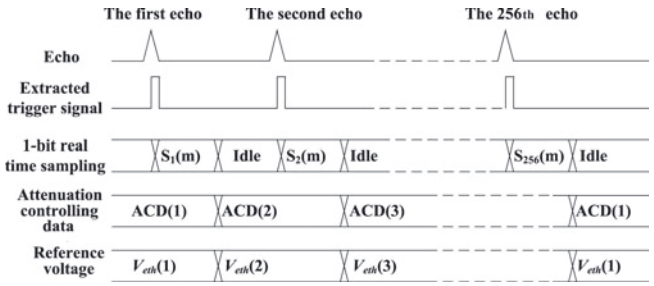

Fig. 5. Timing of the sampling controller.

generally is enough for deep ice detection. Moreover, employing the new variable-gain control method discussed later improves the dynamic range and helps make up, at least in part, for the accuracy limitation.

Similar to the echo signal, the synchronous signal, V_{sin}, is also given an appropriate fixed bias voltage, $V_{\mathrm{sin\_DC}}$ (can be equal to $V_{\mathrm{ein\_DC}}$), and then applied to the positive input of another differential input buffer (Buffer_s). A fixed reference voltage, $V_{\mathrm{sth\_const}}$, is applied to the negative input. When satisfying $V_{\mathrm{sin}} + V_{\mathrm{sin\_DC}} > V_{\mathrm{sth\_const}}$, a short-duration pulse is generated by Buffer_s and sampled by the following DDR sampler. The main logical control unit detects the positive edge of this short pulse and enables 1-bit analog-to-digital conversion, to sample the V_{ein}. This triggering process is similar to the operation of a real-time oscilloscope. Generally, $V_{\mathrm{sth\_const}}$ should be set high enough that only the direct waves which travel along the air–ground interface can trigger the 1-bit analog-to-digital conversion.

Besides controlling the analog-to-digital conversion, the sampling controller also sends 6-bit attenuation-controlling data (ACD) to the attenuator. Because this system employs new sampling technology, conventional time variable-gain controlling methods (Wright and others, 1990; Zamora and others, 2009), in which the gain changes with time, are not suitable here. We employ a new and simply implemented variable-gain controlling method, in which the gain changes with reference voltage, $V_{\mathrm{eth}}(n)$. The result is that a small-amplitude signal obtains larger gain than a large-amplitude signal, which compensates for the smaller amplitude of return signals from more distant objects. Moreover, the changing of the attenuation data is done within a PRF time, resulting in the low switching time requirement for the attenuators. The timing of the sampling controller is shown in Figure 5. The relationship between the reference voltage, $V_{\mathrm{eth}}(n)$, the attenuation-controlling data and the index, n, is shown in Figure 6.

A simulation result is shown in Figure 7. The input signal is one cycle of a 50 MHz sine wave with 100 mV peak-to-peak in 19 ns and one cycle of a 50 MHz sine wave with 10 mV peak-to-peak in 230 ns. This signal is amplified by the proposed variable-gain controlling method and sampled by the new sampling method. The sampling rate is 512 MHz and the quantifying level is 2.3 mV. Figure 7 shows that the small- and large-amplitude sine waves are amplified by about 32 and 14 dB respectively. We conclude that this new variable-gain controlling method is effective and well suited for our application.

Interface

To meet the high-speed data communication requirement between the laptop computer and the IPR, we used a high-speed universal serial bus (USB) interface, which has maximum data transfer rates of >53 Mb s^{-1}, to transfer the IPR control parameters and acquired data. Because the power consumption of the whole receiver is <1.5 W, we can use a laptop computer to provide 5 V power to the receiver via a USB data cable.

ICE-THICKNESS MEASUREMENTS

The transmitter and the receiver of the IPR system were placed in separated well-isolated aluminum boxes (Fig. 8), which were filled with foam to keep the inside temperature of the boxes well above 0°C. Both antennae were placed inside plastic tubes for protection. To ensure the antennae remained straight, the plastic tubes were tied to bamboo. Spacing between the transmitter antenna and receiver antenna was ~2 m.

The measurements for the test were made at Zakharoff Ridge (72°54′3.7″ S, 75°12′36.1″ E). The complete IPR system was pulled by hand across the snow surface from the top of the ridge to the bottom. Typical results are shown in Figure 9. The length of the measured profile is ~2.5 km. We improved signal-to-noise ratio by applying the singular spectrum analysis (SSA) algorithm and envelope detection algorithm (Moore and Grinsted, 2006). The SSA algorithm separates each individual radar trace into orthogonal components. The components that explain most of the original

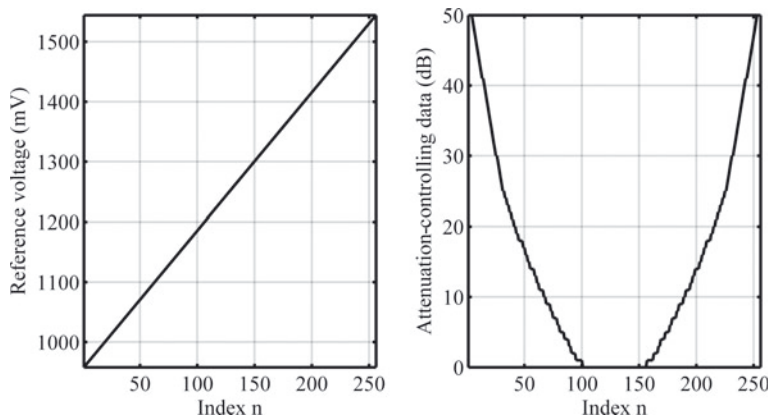

Fig. 6. Relationship between the reference voltage, $V_{\mathrm{eth}}(n)$, the attenuation-controlling data and the index, n.

https://doi.org/10.3189/002214311796405861 Published online by Cambridge University Press

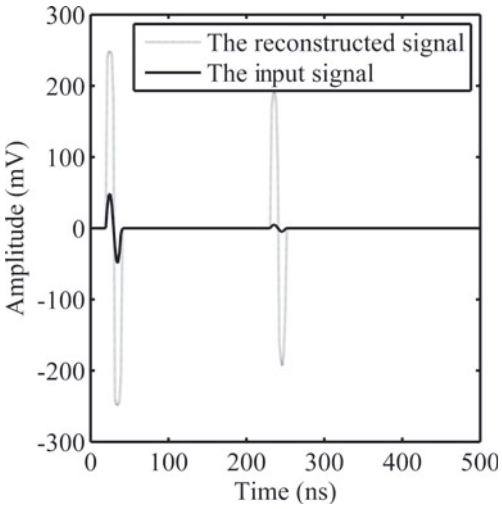

Fig. 7. The simulation result of the receiver. The input signals are one cycle of a 50 MHz sine wave with 100 mV peak-to-peak in 19 ns and one cycle of a 50 MHz sine wave with 10 mV peak-to-peak in 230 ns. The sampling rate is 512 MHz and the quantifying level is 2.3 mV.

trace variance contain mainly physically meaningful signals, while the components with little variance tend to be noise. Furthermore the radargrams can be enhanced by envelope detection of the SSA-filtered data, as this measure of instantaneous energy minimizes the deleterious effects of innumerable phase changes at dielectric boundaries. Additional processing includes geolocating the waveforms, and converting two-way travel (TWT) time to surface elevation and ice thickness. TWT time is converted to distance by assuming a wave speed of $168 \times 10^6\,\mathrm{m\,s^{-1}}$ in cold ice. This assumption will underestimate ice thickness for snow-covered regions of the glacier because the wave speed is faster through snow and firn, and will overestimate ice thickness in regions of the glacier that contain a large amount of liquid water (Macheret and others, 1993). Uncertainty in the estimate of ice thickness comes primarily from uncertainty in the wave speed ($\sim\pm 2 \times 10^6\,\mathrm{m\,s^{-1}}$, which corresponds to ±1.2% of the ice thickness) (Conway and others, 2009).

The depth profile (Fig. 9a) shows reflections with different texture patterns. The maximum measured thickness is ~650 m, with strong signal strength for the bottom reflections. The resolution is ~2.5 m in cold ice. The maximum ice thickness uncertainty is ±3.6 m.

The strong diffuse reflection pattern with TWT time from 0 to 800 ns (Fig. 9b) results from the internal reflections from the firn. Continuous layers demonstrate a depth resolution of 2.5 m. Strong reflections within TWT 2–7 μs in Figure 9a result from the bedrock. Figure 10 shows the raw data waveform and the processed data waveform located at distance 1600 m.

CONCLUSIONS

We describe a low-cost and compact short-pulse IPR system for ice sheets. In contrast to former pulse radar systems, this system has a depth resolution of 2.5 m in cold ice while achieving >650 m penetration range. The bandwidth of the antennas used is ~50 MHz. To achieve a greater penetration range, the peak amplitude of the short pulse is enhanced to ±2500 V. The receiver of the IPR employs asynchronous operation mode, avoiding the cable between the transmitter and receiver. Furthermore, a new sampling technology without integrated analog-to-digital conversion is employed to simplify the structure of the receiver and increase the sampling efficiency. It needs only 256 radar echoes to realize equivalent 8-bit accuracy at 512 MHz sampling rate, independent of the number of sample points. Because of the need for <1.5 W power consumption, the whole receiver system is powered by a laptop computer. The capabilities of the system are indicated by the measurement results. The bedrock at 650 m depth is clearly seen, and the shallow snow accumulation layer in the upper 84 m can be resolved with a resolution of 2.5 m.

Our system may be improved with minor software changes in the FPGA, and is currently being modified to increase sampling rate to 1024 MHz, with a maximum range up to 32 000 ns. In addition, the calculation in Equation (6) is implemented in the FPGA to increase the efficiency of the computer.

We also plan several other modifications, such as (1) using other electronics components to increase the peak amplitude of the pulse, aimed at increasing penetration depth, (2) installing a wireless communication interface to make field measurements more convenient, and (3) investigating additional signal processing methods to raise bed echoes above the noise and clutter. Based on the current radar system, we also plan to develop radars operating at 150, 50 and 10 MHz. We expect to use these IPRs to conduct more measurements on a larger profile extending several km and providing greater detail on ice thickness, internal structure and basal conditions.

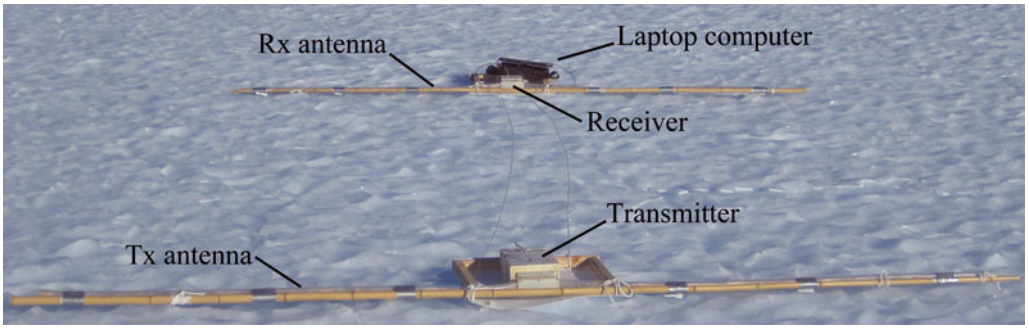

Fig. 8. Configuration for the IPR system on the ice.

https://doi.org/10.3189/002214311796405861 Published online by Cambridge University Press

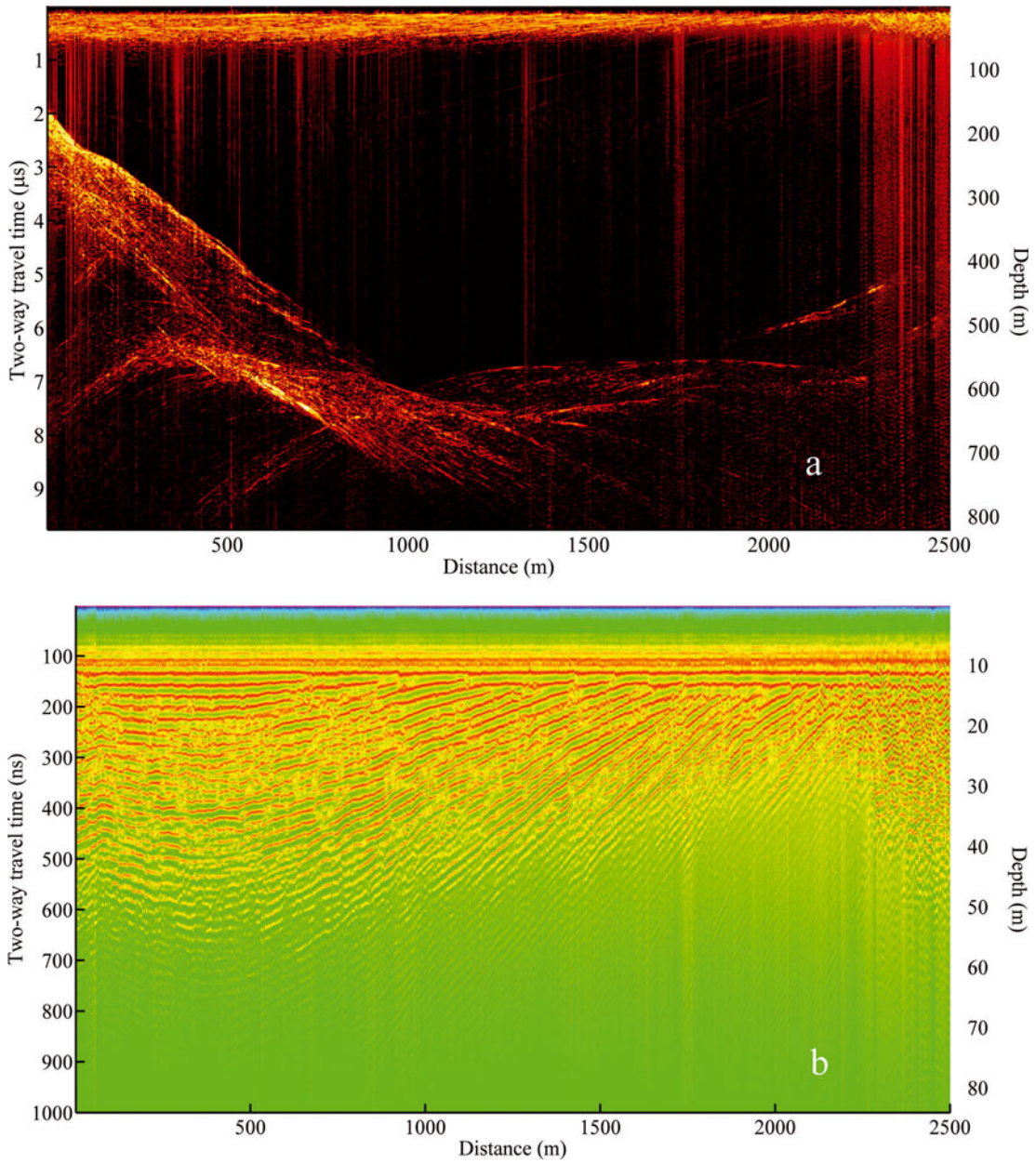

Fig. 9. (a) The complete depth profile at Zakharoff Ridge. (b) The upper 84 m depth profile. The left vertical axis indicates TWT time recorded by the receiver. The right vertical axis indicates depth, which is converted from the TWT time by assuming a wave speed of 168×10^6 m s^{-1} in cold ice. The measured maximum ice thickness is 650 m with uncertainty ±3.6 m.

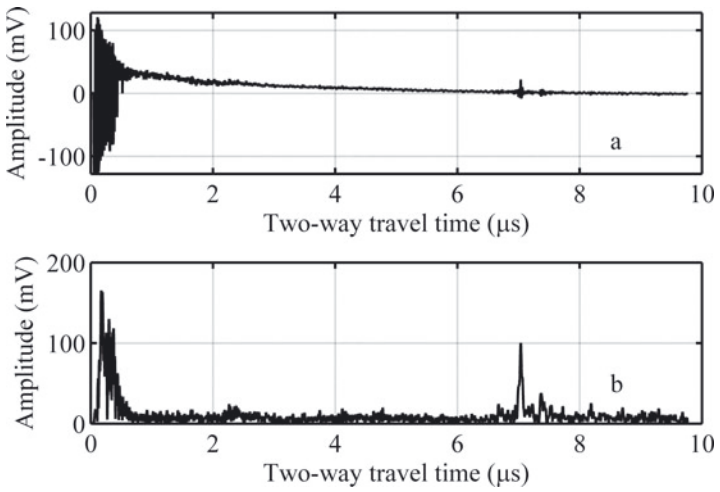

Fig. 10. The recorded waveforms locating at distance 1600 m, (a) from the raw data and (b) from the processed data.

https://doi.org/10.3189/002214311796405861 Published online by Cambridge University Press

ACKNOWLEDGEMENTS

We thank the Polar Office of National Marine Bureau for organization of the 26th China Antarctic Expedition. We thank those who participated in the 5th China Grove Mountains Expedition and assisted in the IPR field survey. This work is supported by the National High Technology Research and Development Program of China (grant No. 2008AA121702-3) and the National Natural Science Foundation of China (grant No. 40976114).

REFERENCES

Bogorodsky, V.V., C.R. Bentley and P.E. Gudmandsen. 1985. *Radioglaciology.* Dordrecht, etc., D. Reidel.

Catania, G.A., T.A. Neumann and S.F. Price. 2008. Characterizing englacial drainage in the ablation zone of the Greenland ice sheet. *J. Glaciol.,* **54**(187), 567–578.

Conway, H., B. Smith, P. Vaswani, K. Matsuoka, E. Rignot and P. Claus. 2009. A low-frequency ice-penetrating radar system adapted for use from an airplane: test results from Bering and Malaspina Glaciers, Alaska, USA. *Ann. Glaciol.,* **50**(51), 93–97.

Jacobel, R.W., B.C. Welch, D. Osterhouse, R. Pettersson and J.A. MacGregor. 2009. Spatial variation of radar-derived basal conditions on Kamb Ice Stream, West Antarctica. *Ann. Glaciol.,* **50**(51), 10–16.

Jones, F.H.M., B.B. Narod and G.K.C. Clarke. 1989. Design and operation of a portable, digital impulse radar. *J. Glaciol.,* **35**(119), 143–148.

Macheret, Yu.Ya., M.Yu. Moskalevsky and E.V. Vasilenko. 1993. Velocity of radio waves in glaciers as an indicator of their hydrothermal state, structure and regime. *J. Glaciol.,* **39**(132), 373–384.

Mingo, L. and G.E. Flowers. 2010. An integrated lightweight ice-penetrating radar system. *J. Glaciol.,* **56**(198), 709–714.

Moore, J.C. and A. Grinsted. 2006. Singular spectrum analysis and envelope detection: methods of enhancing the utility of ground-penetrating radar data. *J. Glaciol.,* **52**(176), 159–163.

Nereson, N.A., C.F. Raymond, R.W. Jacobel and E.D. Waddington. 2000. The accumulation pattern across Siple Dome, West Antarctica, inferred from radar-detected internal layers. *J. Glaciol.,* **46**(152), 75–87.

Sverrisson, M., Æ. Jóhannesson and H. Björnsson. 1980. Radio-echo equipment for depth sounding of temperate glaciers. *J. Glaciol.,* **25**(93), 477–486.

Tsui, J.B.Y. and J.P. Stephens. 2002. Digital microwave receiver technology. *IEEE Trans. Microwave Theory Tech.,* **50**(3), 699–705.

Welch, B.C. and R.W. Jacobel. 2003. Analysis of deep-penetrating radar surveys of West Antarctica. *Geophys. Res. Lett.,* **30**(8), 1444. (10.1029/2003GL017210.)

Welch, B.C. and R.W. Jacobel. 2005. Bedrock topography and wind erosion sites in East Antarctica: observations from the 2002 US-ITASE traverse. *Ann. Glaciol.,* **41**, 92–96.

Welch, B.C., R.W. Jacobel and S.A. Arcone. 2009. First results from radar profiles collected along the US-ITASE traverse from Taylor Dome to South Pole (2006–2008). *Ann. Glaciol.,* **50**(51), 35–41.

Wright, D.L., S.M. Hodge, J.A. Bradley, T.P. Grover and R.W. Jacobel. 1990. A digital low-frequency, surface-profiling ice-radar system. *J. Glaciol.,* **36**(122), 112–121.

Wu, T. and R. King. 1965. The cylindrical antenna with nonreflecting resistive loading. *IEEE Trans. Antennas Propag.,* **13**(3), 369–373.

Zamora, R. *and 8 others.* 2009. Airborne radar sounder for temperate ice: initial results from Patagonia. *J. Glaciol.,* **55**(191), 507–512.

MS received 13 August 2010 and accepted in revised form 17 December 2010